



Direct-Current Nanogenerator Driven by Ultrasonic Waves

Xudong Wang, *et al.*
Science **316**, 102 (2007);
DOI: 10.1126/science.1139366

The following resources related to this article are available online at www.sciencemag.org (this information is current as of April 5, 2007):

Updated information and services, including high-resolution figures, can be found in the online version of this article at:

<http://www.sciencemag.org/cgi/content/full/316/5821/102>

Supporting Online Material can be found at:

<http://www.sciencemag.org/cgi/content/full/316/5821/102/DC1>

This article **cites 22 articles**, 6 of which can be accessed for free:

<http://www.sciencemag.org/cgi/content/full/316/5821/102#otherarticles>

This article appears in the following **subject collections**:

Physics, Applied

http://www.sciencemag.org/cgi/collection/app_physics

Information about obtaining **reprints** of this article or about obtaining **permission to reproduce this article** in whole or in part can be found at:

<http://www.sciencemag.org/about/permissions.dtl>

calculated in the limits of both the diffusive τ_ϕ (solid line, $\tau_\phi^{-1} \propto T$) and ballistic τ_ϕ (dashed line, $\tau_\phi^{-1} \propto T^2$), with $N \cong 10^{-4}$. In fitting the drag variance, we have found τ_ϕ to agree with theory to within a factor of 2 (15), which is typical of the agreement found in other experiments on determining τ_ϕ (24). (The single-layer values of τ_ϕ found from our analysis of the UCF agree with theory to within a factor of 1.5.) Thus, the temperature dependence of the observed drag fluctuations strongly supports the validity of our explanation.

We have observed reproducible fluctuations of the Coulomb drag and demonstrated that they are an informative tool for studying wave properties of electrons in disordered materials, and the local properties in particular. Contrary to UCF, which originate from quantum interference, fluctuations of drag result from an interplay of the interference and e - e interactions. More theoretical and experimental work is required to study their manifestation in different situations. For instance, similarly to the previous extensive studies of the evolution of UCF with increasing magnetic field, such experiments can be performed on the fluctuations of

drag. One of the important developments in the field of Coulomb drag fluctuations can be their study in quantizing magnetic fields, including the regimes of integer and fractional quantum-Hall effects.

References and Notes

- M. B. Pogrebinskii, *Sov. Phys. Semicond.* **11**, 372 (1977).
- P. J. Price, *Physica* **117B**, 750 (1983).
- P. M. Solomon, P. J. Price, D. J. Frank, D. C. La Tulipe, *Phys. Rev. Lett.* **63**, 2508 (1989).
- T. J. Gramila, J. P. Eisenstein, A. H. MacDonald, L. N. Pfeiffer, K. W. West, *Phys. Rev. Lett.* **66**, 1216 (1991).
- U. Sivan, P. M. Solomon, H. Shtrikman, *Phys. Rev. Lett.* **68**, 1196 (1992).
- M. P. Lilly, J. P. Eisenstein, L. N. Pfeiffer, K. W. West, *Phys. Rev. Lett.* **80**, 1714 (1998).
- J. G. S. Lok *et al.*, *Phys. Rev. B* **63**, 041305 (2001).
- A. G. Rojo, *J. Phys. Condens. Matter* **11**, R31 (1999).
- D. Snoke, *Science* **298**, 1368 (2002).
- R. Pillarisetty *et al.*, *Phys. Rev. B* **71**, 115307 (2005).
- M. Yamamoto, M. Stopa, Y. Tokura, Y. Hirayama, S. Tarucha, *Science* **313**, 204 (2006).
- B. N. Narozhny, I. L. Aleiner, *Phys. Rev. Lett.* **84**, 5383 (2000).
- N. A. Mortensen, K. Flensberg, A.-P. Jauho, *Phys. Rev. B* **65**, 085317 (2002).
- I. V. Lerner, *Phys. Lett. A* **133**, 253 (1988).
- The details of the structures, measurements, and the model are available as supporting material on *Science* Online.
- M. Kelllogg, J. P. Eisenstein, L. N. Pfeiffer, K. W. West, *Solid State Commun.* **123**, 515 (2002).
- B. L. Altshuler, P. A. Lee, R. A. Webb, Eds., *Mesoscopic Phenomena in Solids* (North-Holland, New York, 1991).
- A. Kamenev, Y. Oreg, *Phys. Rev. B* **52**, 7516 (1995).
- L. Zheng, A. H. MacDonald, *Phys. Rev. B* **48**, 8203 (1993).
- A.-P. Jauho, H. Smith, *Phys. Rev. B* **47**, 4420 (1993).
- K. Flensberg, B. Y.-K. Hu, A.-P. Jauho, J. M. Kinaret, *Phys. Rev. B* **52**, 14761 (1995).
- B. N. Narozhny, G. Zala, I. L. Aleiner, *Phys. Rev. B* **65**, 180202 (2002).
- B. L. Altshuler, A. G. Aronov, *Electron-Electron Interactions in Disordered Systems*, A. L. Efros, M. Pollak, Eds. (North-Holland, Amsterdam, 1985).
- C. W. J. Beenakker, H. van Houten, in *Solid State Physics*, H. Ehrenreich, D. Turnbull, Eds. (Academic Press, San Diego, 1991).
- We thank I. L. Aleiner, M. Entin, I. L. Lerner, A. Kamenev, and A. Stern for numerous helpful discussions.

Supporting Online Material

www.sciencemag.org/cgi/content/full/316/5821/99/DC1
Materials and Methods

SOM Text
Figs. S1 to S3
References

22 December 2006; accepted 6 March 2007
10.1126/science.1139227

Direct-Current Nanogenerator Driven by Ultrasonic Waves

Xudong Wang, Jinhui Song, Jin Liu, Zhong Lin Wang*

We have developed a nanowire nanogenerator that is driven by an ultrasonic wave to produce continuous direct-current output. The nanogenerator was fabricated with vertically aligned zinc oxide nanowire arrays that were placed beneath a zigzag metal electrode with a small gap. The wave drives the electrode up and down to bend and/or vibrate the nanowires. A piezoelectric-semiconducting coupling process converts mechanical energy into electricity. The zigzag electrode acts as an array of parallel integrated metal tips that simultaneously and continuously create, collect, and output electricity from all of the nanowires. The approach presents an adaptable, mobile, and cost-effective technology for harvesting energy from the environment, and it offers a potential solution for powering nanodevices and nanosystems.

The operation of nanodevices fabricated with one-dimensional nanostructures [such as nanowires, nanotubes, and nanobelts (1–8)] usually requires very low power (9–11), which is provided by an external source, such as a battery that may have to be replaced or recharged regularly. The reliance on an external power source may present a limitation for these systems. Various approaches have been developed for energy scavenging with applications in wireless electronics, such as thermoelectric, piezoelectric thin-film, and vibrational cantilevers (12). We have recently demonstrated an innovative approach for converting nanoscale

mechanical energy into electric energy by piezoelectric zinc oxide (ZnO) nanowire (NW) arrays (13). By deflecting the aligned NWs with a conductive atomic force microscopy (AFM) tip in contact mode, the mechanical energy created by the deflection force was converted into electricity with the use of the piezoelectric properties of the NWs. To improve the power generation capabilities of the system, it is necessary to replace the AFM tip with a simpler source of mechanical energy that can actuate all the NWs simultaneously and continuously. We solved these problems by using ultrasonic waves to drive the motion of the NWs, leading to the production of a continuous current.

The experimental setup is schematically shown in Fig. 1A. An array of aligned ZnO NWs was covered by a zigzag Si electrode coated with Pt. The Pt coating not only

enhanced the conductivity of the electrode, but also created a Schottky contact at the interface with ZnO. The NWs were grown on either GaN substrates (Fig. 1B) or sapphire substrates that were covered by a thin layer of ZnO film (14, 15), which served as a common electrode for directly connecting the NWs with an external circuit. The density of the NWs was $\sim 10/\mu\text{m}^2$, and the height and diameter were $\sim 1.0 \mu\text{m}$ and $\sim 40 \text{ nm}$, respectively. The top electrode was composed of parallel zigzag trenches fabricated on a (001) orientated Si wafer (16) and coated with a thin layer of Pt (200 nm in thickness) (Fig. 1C). The electrode was placed above the NW arrays and manipulated by a probe station under an optical microscope to achieve precise positioning; the spacing was controlled by soft-polymer stripes between the electrode and the NWs at the four sides. The resistance of the nanogenerator was monitored during the assembly process to ensure a reasonable contact between the NWs and the electrode by tuning the thickness of the polymer film. Then the assembled device was sealed at the edges to prevent the penetration of liquid. A cross-sectional image of the packaged NW arrays is shown in Fig. 1D; it displays a “lip/teeth” relationship between the NWs and the electrode. Some NWs are in direct contact with the top electrode, but some are located between the teeth of the electrode. The inclined NWs in the scanning electron microscopy (SEM) image were primarily caused by the cross sectioning of the packaged device. The packaged device was supported by a metal plate that was direct in contact with water contained in the cavity of an ultrasonic generator. The operation

School of Materials Science and Engineering, Georgia Institute of Technology, Atlanta, GA 30332-0245, USA.

*To whom correspondence should be addressed. E-mail: zhong.wang@mse.gatech.edu

frequency of the ultrasonic wave was ~ 41 kHz. The output current and voltage were measured by an external circuit at room temperature.

The experimental design relies on a unique coupling between piezoelectric and semiconducting properties of the aligned ZnO NWs (13, 17, 18). The asymmetric piezoelectric potential across the width of a ZnO NW and the Schottky contact between the metal electrode and the NW are the two key processes for creating, separating, preserving, accumulating, and outputting the charges [see figure 3 in (13)]. A top electrode is designed to achieve the coupling process and to replace the role played by the AFM tip, and its zigzag trenches act as an array of aligned AFM tips (fig. S2 and Fig. 2A). When subject to the excitation of an ultrasonic wave, the zigzag electrode can move down and push the NW, which leads to lateral deflection of NW I. This, in turn, creates a strain field across the width of NW I, with the NW's outer surface being in tensile strain and its inner surface in compressive strain. The inversion of strain across the NW results in an inversion of piezoelectric field E_z along the NW (fig. S1), which produces a piezoelectric-potential inversion from V^- (negative) to V^+ (positive) across the NW (Fig. 2B). When the electrode makes contact with the stretched surface of the NW, which has a positive piezoelectric potential, the Pt metal–ZnO semiconductor interface is a reversely biased Schottky barrier, resulting in little current flowing across the interface. This is the process of creating, separating, preserving, and accumulating charges (13). With further pushing by the electrode, the bent NW I will reach the other side of the adjacent tooth of the zigzag electrode (Fig. 2C). In such a case, the electrode is also in contact with the compressed side of the NW, where the metal/semiconductor interface is a forward-biased Schottky barrier, resulting in a sudden increase in the output electric current flowing from the top electrode into the NW. This is the discharge process.

Figure 2, A to C, shows four possible configurations of contact between a NW and the zigzag electrode. Analogous to the situation described for NW I, the same processes apply to the charge output from NW II. NW III is chosen to elaborate on the vibration/resonance induced by an ultrasonic wave. When the compressive side of NW III is in contact with the electrode, the same discharge process as that for NW I occurs, resulting in the flow of current from the electrode into the NW (Fig. 2C). NW IV, which is short in height, is forced (without bending) into compressive strain by the electrode. In such a case, the piezoelectric voltage created at the top of the NW is negative [see figure 4 in (13)]. Thus, across the electrode–ZnO interface, a positively biased Schottky barrier is formed; hence, the electrons can flow freely across the interface. As a result, electrons flow from the grounded substrate electrode into the NW and then into the top zigzag electrode as the

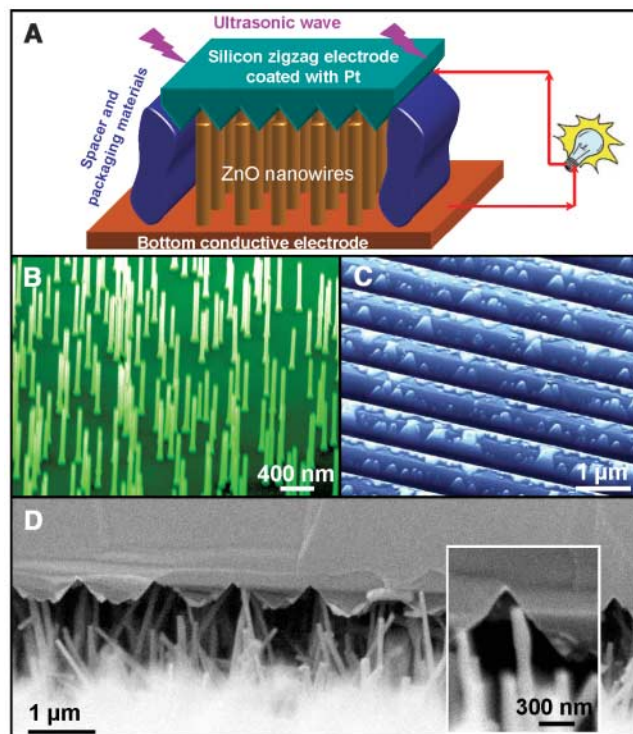
deformation occurs. This discharging process, if substantial, may also contribute to the measured current. In each of the four cases described in Fig. 2, A to C, all of the currents are added up in the same phase.

An equivalent electric circuit is shown in Fig. 2D to illustrate the measurements and outputs of the nanogenerator. The NWs producing current in the nanogenerator are equivalent to a voltage source V_s plus an inner resistance R_i that also contains the contact resistance between the active NWs and the electrode. On the other hand, there are a lot of NWs that are in contact with the electrode but cannot be bent or move freely; thus, they do not actively participate in the current generation, but they do provide a path for conducting current. These NWs are simply represented by a resistance R_w that is parallel to the portion that generates power. A resistance R_c is introduced to represent the contact resistance between the electrode and the external measurement circuit. The capacitance in the system is ignored in the circuit in order to simplify the discussion about dc measurement.

The current and voltage outputs of the nanogenerator are shown in Fig. 2, E and F, respectively, with the ultrasonic wave being turned on and off regularly. A jump of ~ 0.15 nA was observed when the ultrasonic wave was turned on, and the current immediately fell back to the baseline once the ultrasonic wave was turned off. Correspondingly, the voltage signal exhibited a similar on and off trend but with a negative output of ~ -0.7 mV. The negative sign

of the voltage is consistent with the mechanism presented in Fig. 2C. The signal-to-noise ratio of the current is substantially better than that of the output voltage for the following reasons: Because the resistance of the current meter (ideally, zero) plus R_c (20 to 30 ohms) was only $\sim 1/1000$ of R_w when the current was measured, the current generated by the nanogenerator can be safely assumed to be bypassing R_w ; the current path is indicated by a solid blue curve in Fig. 2D, so the measured current is $I_A \approx V_s/(R_c + R_i)$. However, because R_w was very much smaller than the inner resistance of a voltage meter (ideally, infinity) when the voltage was measured, a loop was formed between the power-generating portion of the system and R_w , as shown by a solid pink curve in Fig. 2D. In this case, the current is I_V and the measured voltage V is that across the power-generating portion, $V \approx -V_s R_w/(R_i + R_w)$. During the ultrasonic vibration, for the unstable contacts between the NWs and the electrodes, I_A is affected by the instability of V_s and R_i (but mainly by V_s because R_c is a constant), and V is affected by the instability of V_s , R_i , and R_w . As a result, V has about two times the noise level of I_A , consistent with the observations displayed in Fig. 2, E and F. On the other hand, because the voltages created by all of the NWs are in parallel, the output voltage is effectively the voltage created by one NW; thus, it appears relatively unstable and with a larger noise level than that of I_A (Fig. 2F). Furthermore, the output voltage is naturally smaller than that created by deflecting a NW by AFM, because it is limited

Fig. 1. Nanogenerators driven by an ultrasonic wave. (A) Schematic diagram showing the design and structure of the nanogenerator. Aligned ZnO NWs grown on a solid/polymer substrate are covered by a zigzag electrode. The substrate and the electrode are directly connected to an external load. (B) Aligned ZnO NWs grown on a GaN substrate. The gold catalyst particles used for the growth had been mostly vaporized; thus, the final NWs were purely ZnO with flat top ends. (C) Zigzag trenched electrode fabricated by the standard etching technique after being coated with 200 nm of Pt. The surface features are due to nonuniform etching. (D) Cross-sectional SEM image of the nanogenerator, which is composed of aligned NWs and the zigzag electrode. (Inset) A typical NW that is forced by the electrode to bend.



by the smaller degree of deflection amplitude of the NW, as induced by an ultrasonic wave in comparison to that induced by the AFM tip (13). Finally, the output current is a sum of the currents produced by many NWs. Therefore, the current signal is more stable and continuous, and it has been used to characterize the performance of the dc nanogenerator in this study. The resistance of the entire nanogenerator was also measured with and without turning on the ultrasonic wave (Fig. 2G). The resistance remained very stable at $R = 3.560 \pm 0.005$ kilohms. This measurement indicates that the jump in current could not be due to the variation in resistance, as caused by the vibration of the NWs (19), suggesting that the current signal presented in Fig. 2E was created by the nanogenerator.

The output electricity of the nanogenerator is continuous and reasonably stable. A continuous output current is generated when the ultrasonic wave is turned on, and the current disappears when the wave is turned off (Fig. 3A). The output current is in the nanoampere range. The current signal shows no direct coupling with the frequency of the ultrasonic wave, because the wave frequency is ~ 80 times smaller than the resonance frequency of the NWs (~ 3 MHz) (20). The size of the nanogenerator is ~ 2 mm² in effective substrate surface area. The number of NWs that were actively contributing to the observed output current is estimated to be 250 to 1000 in the current experimental design. The nanogenerator worked continuously for an extended period of time of beyond 1 hour (Fig. 3B).

The experimental design [as presented in (Fig. 1)] has been tested in comparison to the experiments conducted using different materials or configurations. Using the design shown in Fig. 1A, simply by replacing a ZnO NW array with an array of carbon nanotubes (CNTs), no jump in current was observed when the ultrasonic wave was turned on (Fig. 4A). This is because the CNTs are not piezoelectric. In a system with a ZnO NW array but in which the top electrode was replaced with a flat, thin Pt film that totally covered the tips of the NWs (Fig. 4B), no jump in output current was observed. This is because the design does not follow the mechanism of the nanogenerator (fig. S1) (13). A clear jump was observed only when the top electrode was in a zigzag shape and when ZnO NWs were present (Fig. 4C). These experiments may rule out possible contributions from electronic noise and/or measurement error or artifacts in producing the output current, and they consistently support the process proposed in Fig. 2, A to C, for piezoelectric NWs.

In comparison to our previous work (13), our current work has achieved three major objectives: (i) We have replaced the expensive and sophisticated AFM tip with ultrasonic waves/vibrations to induce the elastic deformation and vibration of the NWs, and we have demon-

strated a cost-effective prototype technology for fabricating the nanogenerator. (ii) We have integrated an array of tips into a zigzag electrode for the simultaneous creation, collection, and output of electricity generated by many NWs, establishing the principle for raising the output power. (iii) We have achieved a continuous and fairly stable dc output with this system. The principle demonstrated here has set a platform for harvesting energy from the environment to power in vivo biosensors, wireless and remote sensors, and nanorobots, and it has also established the basis for building zero-power force/pressure sensors.

The number of NWs that was effective for producing output electricity can be estimated

from the output power of the nanogenerator. From our previous study [see supporting online material for (13)], the NW deformed by AFM produced an electric energy of $\Delta E_{\text{AFM}} \sim 0.01$ fJ for each cycle of discharge, which lasted for 0.1 ms; thus, the power generated by one NW was $\Delta W_{\text{AFM}} \sim 0.1$ pW. In the current experimental design, the vibrational amplitude of the NW was much smaller than that of the NW directly deflected by an AFM tip; thus, the output voltage was ~ 1 mV, which is about 5 to 10 times smaller than that received when AFM was used as the deformation tool (13). In this case, the output power of a NW, as driven by ultrasonic wave, would be $\Delta W_{\text{wave}} = 1$ to 4 fW. The output-power volume density per NW is ~ 1 to

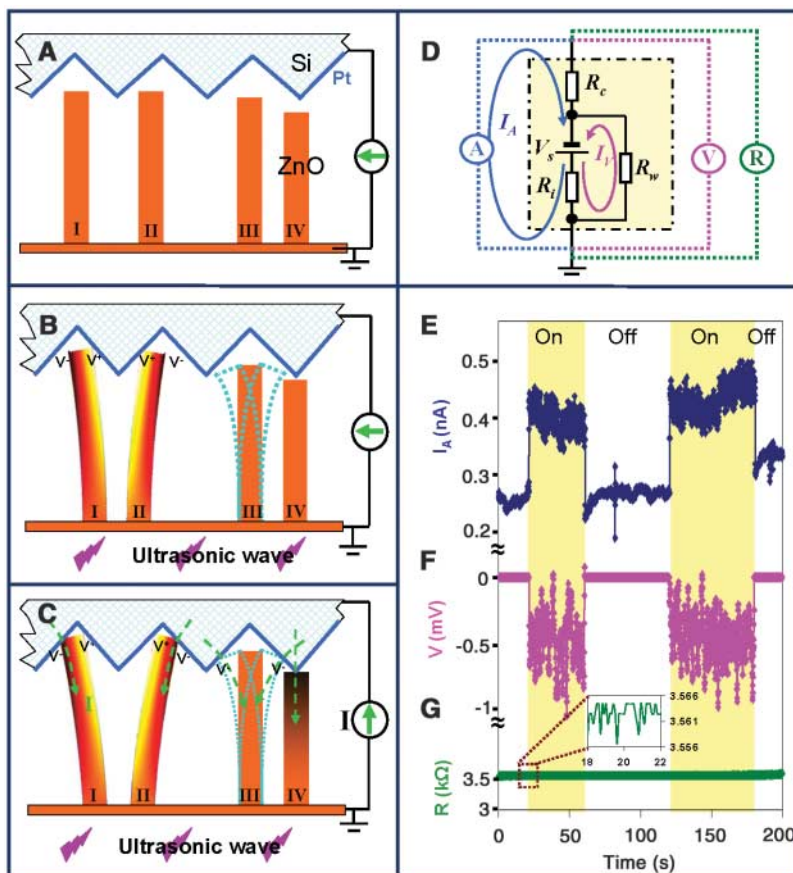


Fig. 2. The mechanism of the nanogenerator driven by an ultrasonic wave. (A) Schematic illustration of the zigzag electrode and the four types of NW configurations. (B) Piezoelectric potential created across NWs I and II under the push or deflection of the electrode, as driven by the ultrasonic wave, but without the flow of current because of the reversely biased Schottky barrier at the electrode/NW interface. NW III is in vibration under the stimulation of the ultrasonic wave. NW IV is in compressive strain without bending. (C) Once the NWs touch the surface of the adjacent teeth, the Schottky barrier at the electrode/NW interface becomes forward-biased, and piezoelectric discharge occurs, resulting in the observation of current flow in the external circuit. (D) Equivalent circuit of the nanogenerator and the setup for measuring the output current I , output voltage V , and resistance R . (E to G) I , V , and R measured with the connections shown in (D), respectively, when the ultrasonic wave was turned on and off purposely. The baseline of the current signal was produced by the electronic measurement system and the interference from the ultrasonic-wave source. Because the voltages created by all of the NWs are in parallel, the output voltage is effectively the voltage created by one NW; thus, it appears to be relatively unstable and with a larger noise level than that of I_A . A pixel averaging was applied for (F). The inset in (G) is an enlargement of the resistance before and after the wave was turned on.

4 W/cm³, which is more than two orders of magnitude higher than that produced by a vibrational microgenerator (21). The output power of the nanogenerator fabricated with a substrate of area = 2 mm² is $W_{\text{wave}} = I_{\Delta}V \approx 1$ pW (Fig. 2, C and D). Therefore, the number of NWs that was active for producing electricity in Fig. 2E was $N = W_{\text{wave}}/\Delta W_{\text{wave}} \approx 250$ to 1000 NWs. As limited by the multiple contacts between the NWs and the electrode in the present design (Fig. 1D), the large majority of the NWs did not produce electricity because of their nonuniformity in height and distri-

bution on the substrate surface; thus, the output current was rather small in the present design. In addition, some of the NWs directly pushed the electrode at the top edges/apexes of the zigzag trenches, preventing the other NWs from reaching and contacting the electrode to produce electricity. These technical difficulties could be overcome by an optimized design to improve nanogenerator efficiency. For example, nanogenerator efficiency could be improved with the use of patterned-tip arrays as the electrode, the designed and patterned growth of high-quality uniform NW

arrays matching the design of the electrode (fig. S2), and an improved packaging technology to keep a precise control on the spacing and alignment between the electrode and the NW arrays. If the area taken by each metal tip is 0.5 by 0.5 μm (fig. S2), the grown density of the NWs is $\sim 10^9/\text{cm}^2$. If one NW produces 10 fW of power by optimizing its size and shape, the output power per unit of area could be 10 μW/cm². The power used to operate a device fabricated with one NW or nanotube is ~ 10 nW (9–11); thus, the nanogenerator built with the NWs grown on an area of 1 cm² could operate up to 1000 of such nanodevices, based on our current study. We anticipate that the performance will be improved by two to three orders of magnitude with improved design and optimization of the nanogenerator (22–23).

Fig. 3. Continuous dc output of the nanogenerator, as characterized by the current signal. (A) Reproducible and highly repeatable current output of the nanogenerator when the ultrasonic wave was turned on and off. (B) Continuous current output of the nanogenerator for an extended period of time. The data are displayed after they were corrected for the background introduced by electronic drift. The baseline of the current signal was produced by the electronic measurement system and the interference from the ultrasonic-wave source. The size of the nanogenerator is ~ 2 mm² in effective substrate surface area.

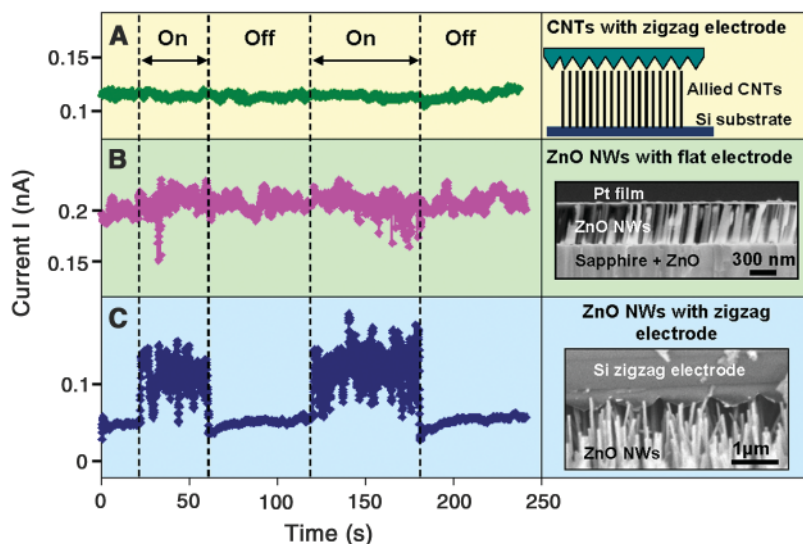
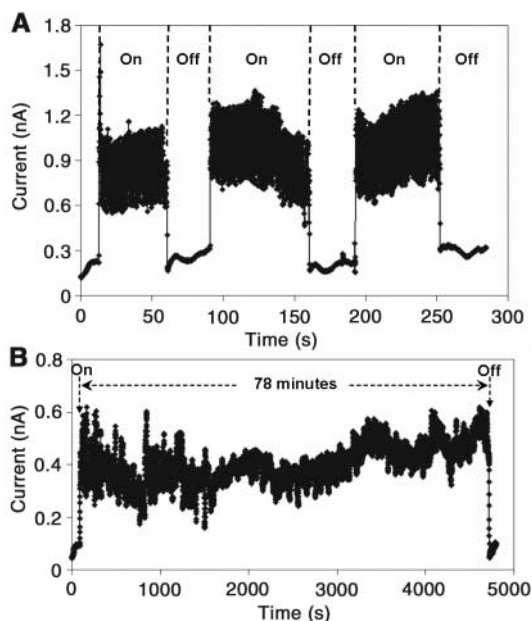


Fig. 4. Output of the nanogenerator with different materials and design configurations. The designs and true-device SEM images are shown on the right-hand side, and the corresponding current curve is on the left-hand side. (A) Nanogenerator based on arrays of CNTs with a zigzag top electrode, showing no jump in current when the ultrasonic wave was turned on. (B) Nanogenerator based on arrays of ZnO NWs but with a flat top electrode, showing no jump in current while stimulated by an ultrasonic wave. (C) Nanogenerator based on arrays of ZnO NWs with a zigzag top electrode, showing a large jump in current when the ultrasonic wave was turned on. The baseline in the current signal was produced by the measurement electronics.

References and Notes

1. F. Patolsky *et al.*, *Science* **313**, 1100 (2006).
2. Y. Li, F. Qian, J. Xiang, C. M. Lieber, *Mater. Today* **9**, 18 (2006).
3. F. Patolsky, C. M. Lieber, *Mater. Today* **8**, 20 (2005).
4. P. Pauzauskis, P. Yang, *Mater. Today* **9**, 36 (2006).
5. A. Javey, J. Guo, Q. Wang, M. Lundstrom, H. J. Dai, *Nature* **424**, 654 (2003).
6. J. W. R. Hsu *et al.*, *Nano Lett.* **5**, 83 (2005).
7. Z. R. Tian *et al.*, *Nat. Mater.* **2**, 821 (2003).
8. Z. W. Pan, Z. R. Dai, Z. L. Wang, *Science* **291**, 1947 (2001).
9. Y. Huang *et al.*, *Science* **294**, 1313 (2001).
10. A. Bachtold, P. Hadley, T. Nakanishi, C. Dekker, *Science* **294**, 1317 (2001).
11. J. Chen *et al.*, *Science* **310**, 1171 (2005).
12. J. A. Paradiso, T. Starner, *IEEE Pervasive Comput.* **4**, 18 (2005).
13. Z. L. Wang, J. Song, *Science* **312**, 242 (2006).
14. X. D. Wang *et al.*, *J. Am. Chem. Soc.* **127**, 7920 (2005).
15. X. D. Wang, C. J. Summers, Z. L. Wang, *Nano Lett.* **4**, 423 (2004).
16. J. Frühauf, S. Krönert, *Microsyst. Technol.* **11**, 1287 (2005).
17. J. H. Song, J. Zhou, J. Liu, Z. L. Wang, *Nano Lett.* **6**, 1656 (2006).
18. X. D. Wang *et al.*, *Nano Lett.* **6**, 2768 (2006).
19. Among the 200,000 NWs on the substrate surface, less than 0.5% were actively creating current. A large percentage of the NWs were serving as current paths between the top and bottom electrodes (Fig. 1D). The resistance introduced by the active NWs was less than 2% of the total resistance, when considering the NWs that were not in contact with the electrodes; thus, it could not produce the large jump in current as observed experimentally.
20. X. D. Bai, P. X. Gao, Z. L. Wang, E. G. Wang, *Appl. Phys. Lett.* **82**, 4806 (2003).
21. P. D. Mitcheson *et al.*, *J. Microelectromech. Syst.* **13**, 429 (2004).
22. P. X. Gao, J. H. Song, J. Liu, Z. L. Wang, *Adv. Mater.* **19**, 67 (2007).
23. Z. L. Wang, *MRS Bull.* **32**, 109 (2007).
24. We thank the Emory Georgia Tech Center of Cancer Nanotechnology Excellence funded by NIH, the Defense Advanced Research Projects Agency, and NSF (grant DMR 9733160) for support. We also thank C. M. Lieber and P. Gao for many stimulating discussions.

Supporting Online Material

www.sciencemag.org/cgi/content/full/316/5821/102/DC1
SOM Text
Figs. S1 and S2

28 December 2006; accepted 1 March 2007
10.1126/science.1139366